JOURNAL OF GEOPHYSICAL RESEARCH, VOL. 113, A10209, doi:10.1029/2008JA013060, 2008

A three-dimensional dynamic kinetic model of the plasmasphere

V. Pierrard[1] and K. Stegen[1]

Received 25 January 2008; revised 23 April 2008; accepted 16 July 2008; published 16 October 2008.

[1] The scientific goal of the present paper is to develop a three-dimensional physical dynamic model of the plasmasphere that is constrained by realistic data. The core of the plasmasphere is obtained from the kinetic exospheric approach assuming a kappa velocity distribution function for the particles. The relative abundance of trapped particles is constrained in such way that the density profiles correspond to Carpenter and Anderson's (1992) observations. The position of the plasmapause is determined by the interchange instability mechanism for the formation of the plasmapause, which is a function of the level of geomagnetic activity. The deformation of the plasmasphere during quiet and disturbed geomagnetic periods is illustrated and compared with the results of other plasmaspheric models and observations of IMAGE and Cluster.

Citation: Pierrard, V., and K. Stegen (2008), A three-dimensional dynamic kinetic model of the plasmasphere, *J. Geophys. Res.*, *113*, A10209, doi:10.1029/2008JA013060.

1. Introduction

[2] The plasmasphere is a region of relatively dense (10–10000 cm^{-3}) but cold (1 eV) plasma, surrounding Earth and extending to distances of about 5 Earth radii (R_E). It is the upward extension of the Earth's ionosphere, getting less and less dense with increasing altitude, and sharing the Earth's corotation [*Lemaire and Gringauz*, 1998]. This rather dynamic region interacts with the ionosphere and other regions of the magnetosphere. Recent observations of the satellites Cluster and IMAGE have provided interesting new features of the plasmasphere and the plasmapause which is its outer edge [*Pierrard*, 2006; *Darrouzet et al.*, 2006].

[3] Models of the plasmasphere and plasmapause that have been developed in the past are mainly empirical models, i.e., on the basis of average density measurements and in situ whistler observations. One of the most popular empirical models for the equatorial electron density has been developed by *Carpenter and Anderson* [1992] (CA92) on the basis of near equatorial ISEE 1 radio measurements and whistlers observations. A dynamic global core plasma model (DGCPM) was also used to investigate the effects of subauroral ion drift (SAID) events on the formation of trough density profiles in the outer plasmasphere during periods of high magnetic activity [*Ober et al.*, 1997]. More recently, *Gallagher et al.* [2000] developed the global core plasma model (GCPM) providing plasmaspheric density as a function of geomagnetic and solar conditions. The GCPM is a combination of empirical density models including the International Reference Ionosphere (IRI) of *Bilitza et al.* [1993] at low altitudes, and a linear least square fit to the logarithm of plasmaspheric densities measured by the DE1/RIMS (Dynamics Explorer 1/Retarding Ion Mass Spectrometer) instrument. CRRES observations were also used to develop an empirical model of the plasmasphere and trough density [*Sheeley et al.*, 2001].

[4] *Reinisch et al.* [2001] and *Huang et al.* [2004] developed an empirical model to describe the two-dimensional density distribution in the inner magnetosphere on the basis of recent observations of the radio plasma imager (RPI) on the IMAGE satellite. They adjust a set of constant parameters characterizing mathematical functions to fit the electron density distribution they determined experimentally from their RPI measurements during successive passes of IMAGE in the plasmasphere. The mathematical functions are not related to any theoretical models of field aligned plasma density distributions on the basis of physical grounds.

[5] The FLIP (Field Line Interhemispheric Plasma) model [*Tu et al.*, 2003] has also been used to analyze the RPI/IMAGE observations of electron density along field lines. This model solves the equations of continuity, momentum and energy conservation of the particles in both hemispheres. The calculated densities in the regions far from the equator were much lower than observed values, while good agreement was obtained in the equator.

[6] Another physics-based model of the plasmasphere has been developed by *Webb and Essex* [2004]. Their three-dimensional Global Plasmasphere Ionosphere Density (GPID) model uses a dynamic diffusive equilibrium approach within each magnetic flux tube. This advanced theoretical model constitutes a significant improvement compared to the purely empirical models of the plasmasphere, but it requires more computer resources. Let us note also the modeling efforts of the plasmapause by *Goldstein et al.* [2005a] developing a magnetospheric model of the subauroral polarization stream (SAPS) electric potential. Physics-based models of the plasmasphere are reviewed by V. Pierrard et al. (Physics-based models of the plasmasphere, submitted to *Space Science Reviews*, 2008).

[7] In the present paper, we develop a three-dimensional physical model of the plasmasphere on the basis of the

[1]Belgian Institute for Space Aeronomy, Brussels, Belgium.

0148-0227/08/2008JA013060$09.00

kinetic formulation for a rotating ion exosphere. It is indeed crucial to develop improved physical models of the plasmasphere to better understand the mechanisms affecting the plasmasphere number density and the plasmapause position. The evaluation of the plasmaspheric electron content interests GPS for instance. Moreover, recent studies indicated that the core plasmasphere distribution and specifically the position of the plasmapause have a dynamic relationship with ring current and radiation belt populations [*Baker et al.*, 2004; *Goldstein et al.*, 2005b].

[8] The family of kinetic models described below are characterized by field aligned density distributions ranging between two extremes: (1) diffusive equilibrium (DE), a state of saturation where a full population of trapped particles is considered, and (2) exospheric equilibrium (EE), which corresponds to a kind minimal density distribution where magnetic flux tubes are fully depleted of their trapped particles. In this EE model, the population of particles is ideally formed of ballistic particles (emerging from below an exobase level, but with insufficient kinetic energy to reach the equatorial plane), and all the particles which can fly from the exobase over the equatorial region into the conjugate hemisphere. In the EE model, there are no "trapped" particles with mirror points above the exobase altitudes, i.e., there are no particles with pitch angles outside the loss and source cones.

[9] The present family of kinetic models described in section 2 are characterized by plasma density distributions which are intermediate between these two extremes: the concentration of trapped particles (i.e., particles whose pitch angles are outside the loss and source cones) is adjusted so that the number densities at low altitudes and in the equatorial plane in all geomagnetic flux tubes correspond to the averaged values determined from various sets of observations.

[10] All these kinetic models are in hydrostatic equilibrium, i.e., there is no field aligned bulk flow of particles from one hemisphere to the other. Each species of particle is treated separately and characterized by its own velocity distribution functions (VDF), $f_f(\mathbf{v}, \mathbf{r}, t)$. In the following models, we use the Kappa (i.e., Lorentzian) VDF [*Pierrard and Lemaire*, 1996]. This generalizes the Maxwellian functions when the population of suprathermal particles is enhanced in the tail of the VDF, as often observed in actual magnetospheric and solar wind plasmas [*Maksimovic et al.*, 1997].

[11] The physical models proposed below are analytical, and consequently they are rather easy to implement: they do not require large computer resources. Therefore, the kinetic models of the plasmasphere described below are fairly portable. Furthermore, unlike other empirical models, they incorporate major physical features that determine the density distributions in flux tubes at high altitudes.

[12] Our kinetic models take into account the rotation of the plasmasphere as well as the level of geomagnetic activity that determines the position and width of the plasmapause region. The erosion of the plasmasphere during geomagnetic storms and substorms, as well as its refilling after such events, is also implemented in our kinetic models.

[13] The results of our kinetic models are compared with observations as well as with results from alternative empirical models in section 4.

2. Description of the Kinetic Models

2.1. Exospheric Approach

[14] In the exospheric approach, it is assumed that above a certain altitude called the exobase the motion of charged particles is determined only by the external forces: gravitation, electric force, and Lorentz force. Collisions between particles of the same species or with other atoms, ions or electrons are ignored above the exobase where the Knudsen number is considered to be small. We assume the velocity distribution function (VDF) of the particles to be given at the exobase r_0. The VDF at any higher altitude is determined according to Liouville's theorem as in the rotating ion exosphere models of *Lemaire* [1976] for Maxwellian VDFs, and in the work of *Pierrard and Lemaire* [1996] for Kappa VDFs.

[15] The exobase altitude is defined as the level where the mean free path of particles of average energy is equal to the ionospheric density scale height: it is the altitude where the Knudsen number for these particles becomes equal to unity. The exobase altitude is assumed to be the same in both hemispheres and equal to 2000 km. It is also postulated that the kappa VDFs of all particle species are identical in both hemispheres. This implies that the models developed here are symmetric with respect to the equatorial plane.

[16] Four classes of trajectories exist according to the kinetic energy and pitch angle of the particles. The different classes of particles are represented on Figure 1 in the plane of the velocities parallel (v_{parallel}) and perpendicular (v_{perp}) to the magnetic field lines.

[17] 1. The class A represents the escaping particles: they have enough energy to fly over the equatorial plane and penetrate into the conjugate hemisphere. These particles have a positive v_{parallel}. They have pitch angles within the loss cone and are represented in Figure 1 by the red shaded area.

[18] 2. The class B corresponds to the incoming particles emerging from the conjugate hemisphere and having pitch angles in the loss cone. These particles have a negative v_{parallel} and are represented by the blue shaded area.

[19] 3. The class labeled D corresponds to the ballistic particles emerging from below the exobase that have not enough energy to escape and return to the same hemisphere. Their pitch angles are ranging between 0° and 180°. For this class, v_{parallel} is symmetric with respect to upward and downward directed velocities. It is shaded in green.

[20] 4. The classes C and E correspond to the trapped particles that have two mirror points above the exobase level. Their pitch angles are outside the source and loss cones. The trapped particles with mirror points in opposite hemispheres are represented by the area shaded in purple (C). Those with mirror points in the same hemisphere are represented in yellow (E).

[21] The analytic expressions of the lowest moments of a Lorentzian (Kappa) VDF (the number density, flux, parallel and perpendicular temperature and heat flux) have been

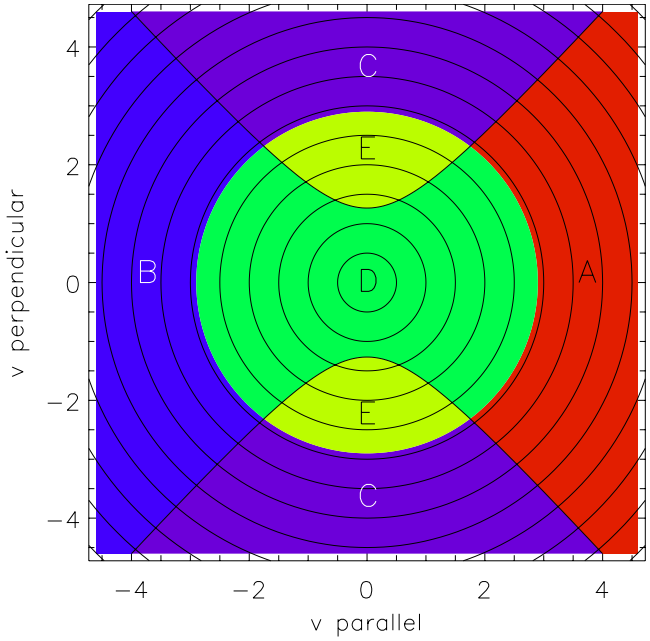

Figure 1. The different classes of orbits along closed field lines represented in the velocity plane. A, escaping particles; B, incoming particles; C, trapped particles with mirror points in two different hemispheres; D, ballistic particles; E, trapped particles with mirror points in the same hemisphere.

calculated separately for each class of particles along open field lines by *Pierrard and Lemaire* [1996]. Appendix A gives the expressions corresponding to the number density along closed field lines for the diffusive (equation (A14)), exospheric (equation (A15)) and constrained (equation (A19)) models. The formulae for Maxwellian VDFs are recovered by letting the index kappa tend to infinity. The analytical expressions of the model constitute a great advantage over solutions obtained by integrating nonlinear transport equations.

[22] Models in diffusive equilibrium (DE) contain a full population of all classes of particle and correspond to equation (A14). *Pierrard and Lemaire* [2001] indicated that such DE models are not satisfactory ones, since their equatorial number density decreases too slowly with the radial distance compared to what is generally observed by whistler observations, as well as by in situ measurements of OGO5, DE-1, ISEE-1, AKEBONO, ACTIVNY, APEX, and INTERBALL. Models in exospheric equilibrium (EE) contain no trapped particles of classes C and E and correspond to equation (A15). Their density profiles decrease faster with the equatorial distance than actually observed during quiet periods. This is the reason why we consider an intermediate kinetic model of the plasmasphere wherein the classes of trapped particles are partially depleted, instead of being fully depleted as in the earlier EE models.

[23] Such constrained models (CM) are adjusted to fit empirical observations and correspond to equation (A19). In the kinetic model of the equatorial density in the plasmasphere by *Pierrard and Lemaire* [2001], the population of the classes C and E was adapted to obtain a specific radial profile for the number density of the plasmaspheric electrons in the geomagnetic equatorial plane. As given by *Pierrard and Lemaire* [2001], the fraction η of trapped particles is here adjusted in order to fit the calculated equatorial density to the observed density profile determined by *Carpenter and Anderson* [1992] from ISEE-1 observations in the equatorial region of the plasmasphere. This experimental density profile corresponds to average equatorial density profiles observed after a series of successive quiet days of low geomagnetic activity conditions. This observed profile is given by equation (A20).

[24] The fraction of trapped particles $\eta(r_{eq})$ that has to be added to the EE model is given by equation (A18). It is a decreasing function of r_{eq}, the equatorial distance of the dipole field line. Such a decrease of $\eta(r_{eq})$ is expected, since the frequency of collisions decreases with the radial distance and therefore with r_{eq} or L. Furthermore, we assume that the fraction η of trapped particles along the different field lines is only a function of r_{eq} (or of L, or of invariant latitude Λ). We assume that the exobase densities and temperatures characterizing the exobase VDF in both hemispheres are independent of the invariant latitude of the dipole magnetic field lines and of its magnetic local time. Although these assumptions can easily be relaxed, we adopt these assumptions in the present kinetic model in order to minimize the number of free adjustable model parameters. Furthermore, for a similar reason, we assume that the values of the kappa indexes characterizing the tail of the VDFs do not change with the invariant latitude (or with r_{eq}) nor with the magnetic local time (MLT) of the dipole magnetic field lines. Of course, these simplifications could be relaxed in more sophisticated assimilation models of the plasmasphere involving MLT variations. Seasonal and solar sunspot variations are taken into account in the fit of the average profile of CA92 given in equation (A20).

[25] *Pierrard and Lemaire*'s [2001] kinetic equatorial model has been extended here to give field-aligned plasma distributions. It constitutes therefore the core of the three-dimensional plasmaspheric model. In this simple version, we assume that the magnetic field is a dipole and that its field lines are given by $R = L\cos^2 \lambda$, where R and λ are respectively the radial distance (in Earth radii) and the magnetic latitude of the points along the field line whose McIlwain parameter is L.

[26] For the sake of simplicity, we assume in this kinetic model that the exobase altitudes (h_0), the exobase electron and proton densities (n_0), as well as the exobase electron and ion temperatures ($T_{0,e}$ and $T_{0,p}$) are equal in both hemispheres. The kappa indexes (κ_e and κ_p) of the electrons and ions Lorentzian VDFs are also the same in both hemispheres, and independent of r_{eq} and of the magnetic local time.

[27] The core of the constrained plasmaspheric model is represented on Figure 2 assuming κ_e and $\kappa_p = 100$ and that the exobase temperatures of electrons and protons are equal to 3000 K in both hemispheres. The exobase altitude is also assumed to be identical in northern and southern hemispheres (2000 km). The same values of these parameters κ, $T(r_0)$, and r_0 are used in all DE, EE, and CM models presented in Figures 2, 3, and 4a of this paper.

[28] Note that because the CA92 model does not give the number density below $L = 2\ R_E$, this low-altitude region of the plasmasphere has to be complemented by another model for the equatorial plasma distribution. IRI ionospheric

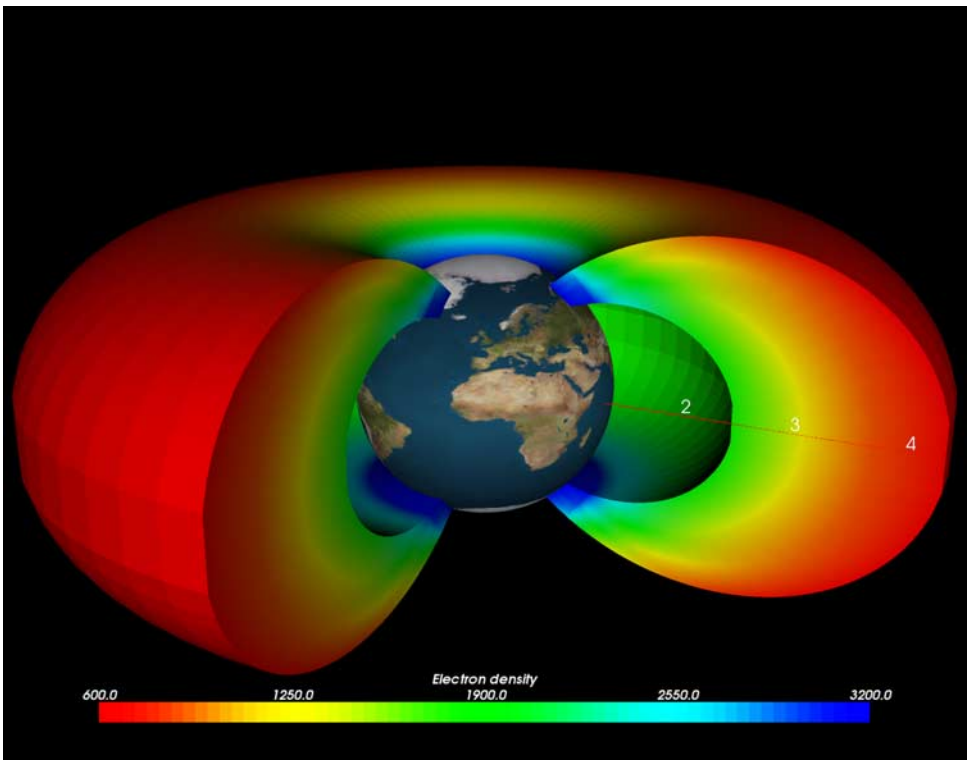

Figure 2. Kinetic model of the plasmasphere in three dimensions obtained by assuming a fraction of trapped particles so that the geomagnetic equatorial profile corresponds to that observed by *Carpenter and Anderson* [1992].

model is only valid below 700 km and cannot be used to fit the range of altitudes up to 13000 km. But other empirical models, like GCPM [*Gallagher et al.*, 2000] for instance, can be used to constrain the model to observed profiles in these regions. GCPM based on DE1 observations and on IRI model for the ionosphere covers a larger range of inner L.

2.2. Rotation of the Plasmasphere

[29] In the present paper, the kappa model of the plasmasphere is generalized in three dimensions by calculating the VDF along the different flux tubes. By adding the corotation and the convection velocity depending on the geomagnetic activity level, the model becomes also dynamic. Indeed, our kinetic model of the plasmasphere takes also into account the effects of the rotation of the plasmasphere (see equation (A24) and equation (A30)). To include the rotation of the Earth in the kinetic model, the centrifugal force is added to the gravitational force and to polarization electric force, as presented in Appendix A. Because of the rotation or convection, any model in diffusive equilibrium (DE) has a minimum density where the magnetic field lines traverse the Zero Parallel Force Surface (ZPFS) [*Lemaire*, 1976, 1989]. This virtual ZPFS is the locus of points where the sum of the gravitational and inertial (centrifugal) forces has a vanishing component along magnetic field lines. The closest points of approach from Earth of this ZPFS are located in the equatorial region of the magnetosphere. When the rate of rotation is equal to the angular velocity of the Earth, the ZPFS intersects the equatorial plane along a circle whose radius is equal to 5.78 R_E. The equatorial distance of the ZPFS is then equal to $L_c = 5.78\ R_E$, i.e., a factor $(3/2)^{1/3}$ smaller than the geosynchronous radius: $L_o = 6.6\ R_E$. The ZPFS is represented by the black line on Figure 3. Figure 3 also shows the number density of a Lorentzian kinetic model with $\kappa = 100$ in diffusive equilibrium. Since the index κ is large, this model is very close to the Maxwellian model in diffusive equilibrium. The minimum of density marks the position of the plasmapause.

[30] Above the Zero Parallel Force Surface located at $L = 5.78\ R_E$ for plasma corotation, the plasma density distributions become unstable because the centrifugal force becomes larger than the gravitational force. Any corotating equatorial plasma density distribution in diffusive equilibrium has a minimum value at $R_{eq} = 5.78\ R_E$. When the rate of angular rotation is larger than that of the Earth, the ZPFS intersects the equatorial plane closer to the Earth. This intersection can be determined by using a convection electric field model like McIlwain's E5D model. This is the magnetospheric E field model used in the present model to determine the equatorial position of the plasmapause, as explained in the next section.

2.3. Determination of the Plasmapause Position

[31] Like in simulations by *Pierrard and Cabrera* [2005], we consider that the plasmapause is the result of the interchange motion becoming unstable along the innermost geomagnetic field lines tangent to the ZPFS [*Lemaire*, 1989]. When the angular rotational speed of the magnetospheric plasma is occasionally enhanced, the minimum equatorial distance of the ZPFS is reduced. For instance, the ZPFS becomes equal to 2.8 R_E for a factor 3 of the angular rotational speed.

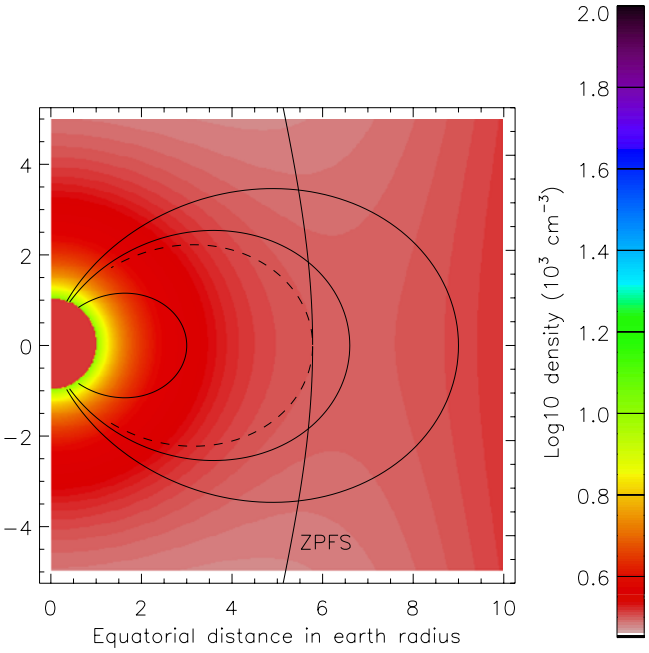

Figure 3. Number density of a kinetic model in diffusive equilibrium (DE) with $\kappa = 100$. Above the Zero Parallel Force Surface (ZPFS) located at $L = 5.78$ R_E for plasma corotation, the plasma density distribution becomes unstable.

[32] The plasmapause develops first in the equatorial region, and subsequently at lower altitudes along the magnetic field lines tangent to the ZPFS. Inward shifts of the ZPFS occur during substorm events, when the magnetospheric convection velocity is significantly enhanced in the midnight and postmidnight MLT sectors. The *Kp*-dependent empirical electric field model E5D [*McIlwain*, 1986] is used in our dynamic simulations to determine the convection velocity, and ultimately the position of the plasmapause. The value of the *Kp* index increases during substorm events and enhances the convection rate in the night MLT sector. This leads to an inward motion of the ZPFS in the MLT sector and therefore the peeling off of the plasmasphere close to Earth.

[33] Other magnetospheric convection electric field models are available in the literature and some of them have been used to determine the positions of the plasmapause by *Pierrard et al.* [2008]. Among all most popular electric field models tested by these authors (Volland-Stern, E5D and Weimer), it happens that the E5D model offers the results that were in slightly closest best agreement with the observations from IMAGE for the cases examined in their comparative study. Note that the model considers the observed variations of *Kp* to determine the variations of the convection electric field using an empirical model on the basis of averaged observations. It is possible inversely to determine the actual convection electric field from plasmapause observations.

[34] A new sharp gradient is formed in the equatorial plasma density distribution where and when the ZPFS shifts closest to Earth during the inward motion of a substorm injection boundary. To determine the position where the new plasmapause is formed, we track the motion of underdense plasma elements released every 10 min in the premidnight MLT sector at an arbitrary radial distance ($R = 4$–7 R_E). Because of the buoyancy force, all plasma elements whose density is smaller than the background density (assumed to be given by the CA92 model), migrate toward the asymptotic trajectory where the radial components of the gravitational and centrifugal accelerations balance each other [*Lemaire and Gringauz*, 1998]. The point of tangency of these drift paths with the electric equipotential surfaces of the convection *E* field model is determined. This minimum radial distance of the ZPFS is then reduced by the factor of $3^{2/3}$, to determine uniquely the place where interchange

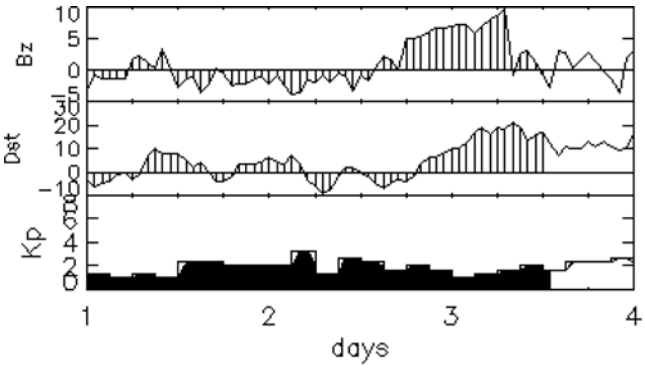

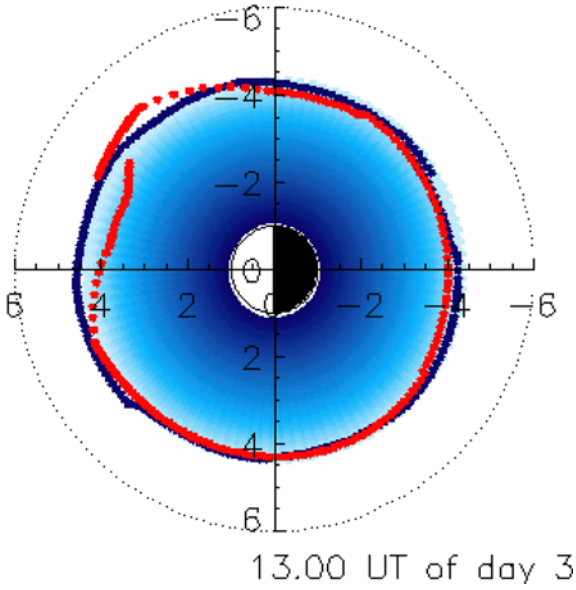

Figure 4a. Results of the dynamic kinetic model. (top) B_z, *Dst*, and *Kp* index from 6 June 2001 at 0000 UT to 8 June 2001 at 2400 UT. (bottom) The blue shading is proportional to the logarithm of the plasma density in the geomagnetic equatorial plane at 1300 UT on 8 June 2001. The number density inside the plasmasphere decreases according to the empirical model of *Carpenter and Anderson* [1992] (CA92). The blue dots correspond to the contemporary outer edge of the plasmasphere. The red dots represent the positions of the vestigial plasmapause that was formed at an earlier enhancement of the convection electric field. They correspond to the inner edge of the plasmapause when they are located closer to the Earth than the black dots.

motion is becoming unstable and peeling off the plasmasphere (see the equations of Appendix A for the determination of plasmapause position). Once the minimum radial distance for the ZPFS has been determined as indicated above, the MHD drift velocity, $\mathbf{E} \times \mathbf{B}/B^2$, is used to calculate the positions of the plasmapause in following MLT sectors and at later UT (see equation (A29) and (A30)).

[35] The dynamic simulations of plasmapause formation that have been published by *Pierrard and Lemaire* [2004] on the basis of this scenario predicted positions of the plasmapause successfully confirmed by EUV/IMAGE observations [*Pierrard and Cabrera*, 2005; *Pierrard*, 2006]. Indeed, the model reproduces quite well the formation of plumes often observed during periods of enhanced geomagnetic activity. The results of these simulations have also been successfully compared with observations from Cluster and IMAGE missions by *Dandouras et al.* [2005], *Pierrard and Cabrera* [2006], and *Schaefer et al.* [2007].

[36] The dynamic code that calculates the position of the plasmapause can be run on the space weather portal (by going to www.spaceweather.eu, then to model access, and finally to plasmapause). To run a simulation, a single input parameter is required: the start date. The code calculates the positions of the plasmapause versus MLT every hour UT during that given day using the successive values of *Kp*.

3. Example of Simulations

[37] An example of the plasmaspheric density obtained in the geomagnetic equatorial plane with the kinetic model on 8 June 2001 is illustrated on Figure 4a. This date has been chosen because there are observations of Cluster/WHISPER, IMAGE/EUV, and RPI instruments to compare with. It is a relatively quiet period, since the maximum *Kp* index during the previous 48 h is 3^+. Figure 4a (top) illustrates the values of the Northward component of the interplanetary magnetic field (B_z in nT), the disturbance storm time index (*Dst* in nT), and the values of the geomagnetic activity index *Kp* from the beginning of 6 June 2001 to the end of 8 June 2001. Because of the small variations of *Kp*, the plasmasphere found with our model is almost circular and rather extended (Lpp > 4 R_E). Figure 4a shows the plasmapause obtained by our dynamic model with equations (A28) and (A30) in the geomagnetic equatorial plane on 8 June 2001 at 1300 UT. The equatorial number density inside the plasmasphere is obtained with the CM model (equation (A19)) constrained to the CA92 density profile (equation (A20)) prolonged at low radial distances and using the same parameter values as in Figure 2. The number density decreases with the distance as illustrated by the decreasing blue shading.

[38] We started the simulation more than 2 days earlier, i.e., on 6 June 2001, in order to take into account the temporal evolution of the plasmapause over a period longer than 24 h. The red dots correspond to the (vestigial) plasmapause formed during the first day (from 6 June 2001 at 1300 UT to 7 June 2001 at 1300 UT). The blue dots correspond to the most recent plasmapause, determined by the *Kp*-dependent variations of the convection electric field E5D during the second day (from 7 June 2001 at 1300 UT to 8 June 2001 at 1300 UT). Since observed *Kp* is slightly decreasing, the newest plasmapause (black dots) is formed at larger radial distances than the vestigial plasmapause (red dots) in almost all MLT sectors. When and where the red dots are closer to Earth than the black dots, the red dots correspond to the inner edge of the refilling region, while the blue dots correspond to the outer edge of the contemporary plasmasphere. Plasma refilling is expected in this intermediate region. Quite long characteristic times (ranging from one to several days, depending on *L*, are necessary to refill emptied flux tubes.

[39] Especially during refilling periods corresponding to periods of decreasing values of *Kp*, the simulations have to be started a few days earlier the requested date, in order to account for the existence of a vestigial plasmapause and the time delay needed to fill the depleted layers of the outer region of the plasmasphere. On 8 June 2001 at 1300 UT, the inner edge of the plasmapause is found at about 4 R_E and the outer edge near 4.5 R_E in noon MLT sector. In the present case, we consider that the plasma density varies linearly between the inner and outer edges of the refilling region.

[40] On 8 June 2001 at 1300 UT, there are exploitable observations from the EUV (Extreme Ultra Violet) instrument on board the satellite IMAGE (Imager for Magnetopause-to-Aurora Global Exploration). This image is illustrated in Figure 4b. It is an intensity map of the 30.4 nm emissions of Helium ions integrated along the line of sight. It is projected in the geomagnetic equatorial plane in the SM coordinate system to display the plasmapause cross section from over the North Pole like in our simulations. The plasmasphere corresponds to the region in green surrounding the Earth. The plasmapause corresponds to the sharp edge where the brightness of 30.4 nm He^+ emissions drops drastically. This boundary is illustrated by a white line corresponding to a threshold equal to 40% of the maximum light intensity. The observed plasmasphere is quite extended in radial distance. The plasmapause is located around 4.5 R_E and does not exhibit amplitude variations as function of MLT. In the morning MLT sector, the plasmapause is slightly closer to the Earth than in the earlier local time sectors.

[41] The situation is quite different 2 days later, after the geomagnetic substorm of 9 June 2001. Indeed, as illustrated in Figure 5a (top) the evolution of B_z, *Dst*, and *Kp* from 8 June 2001 at 0000 UT to 10 June 2001 at 2400 UT, the geomagnetic activity index *Kp* increased significantly on 9 June 2001 and reaches a maximum $Kp = 6^-$. Like for most substorm events, this increase of *Kp* is associated to a southward turning of the interplanetary magnetic field B_z, as well as a decrease of *Dst* index. Figure 5a illustrates the plasmapause predicted by our model on 10 June 2001 at 0800 UT. The *Kp* increase resulted in the erosion of the plasmasphere, with a sharp plasmapause created closer to the Earth and the formation of a plume rotating with the plasmasphere in the eastward direction. Such plumes are mostly formed during geomagnetic storms and substorms [*Pierrard and Cabrera*, 2005]. As a consequence of the *Kp* enhancement, the plasmapause (blue dots) appears at reduced radial distances. The plasmapause is rather sharp during such periods of enhanced geomagnetic activity since the inner and outer edges of the plasmapause region are then located at the same radial distances in the model. The vestigial plasmapause (red dots) lasts only following a maximum value of the *Kp* index, i.e., after the end of the

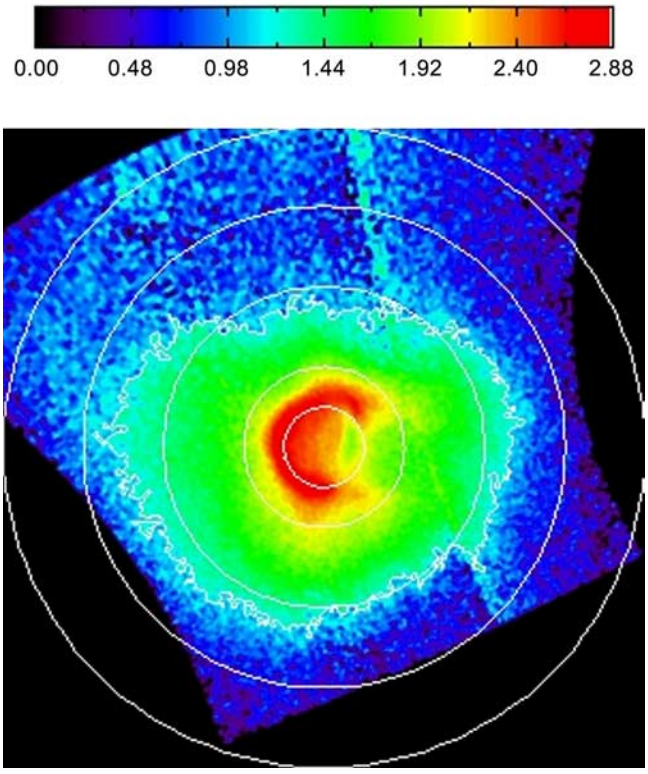

Figure 4b. Observation of EUV/IMAGE on 8 June 2001 at 1300 UT, projected in the geomagnetic equatorial plane. The white circles correspond respectively to $L = 2$, 4, 6, and 8 R_E.

substorm events and corresponds then in our simulations to the inner edge of the plasmapause. A shoulder is then formed in the morning side of the plasmapause. A plume develops also in the duskside plasmasphere during this period, as often observed in association with geomagnetic storms or substorms. It can be seen in Figure 5a that such a plume is indeed predicted by our dynamic model at 0800 UT in the dusk MLT sector.

[42] The EUV/IMAGE observation obtained on 10 June 2001 at 0805 UT is shown Figure 5b. As predicted by our dynamic model, a plume is observed in the dusk sector, as well as a shoulder which is clearly visible although its location is 1 h ahead in MLT. Such discrepancy can of course easily be accounted for because of the rather poor time resolution (3 h) of the *Kp* index which controls the E5D electric field model used in our simulations.

[43] The observed equatorial distance of the plasmapause is around $L = 3$ R_E, which is a little bit closer to Earth than what is found with our model in the night sector. This discrepancy can be attributed to the inherent limitations of the E5D model. Several other plasmapause positions found with similar interchange simulations compared to EUV observations have been presented by *Pierrard and Cabrera* [2005, 2006].

4. Comparison With Other Models and Observations

4.1. Equatorial Profiles

[44] In the present section, the equatorial density profile predicted by our kinetic model for 8 June 2001 is compared with the results of other models and observations. The equatorial profile of our kinetic CM model is obtained by equation (A19)) by including an adjusted fraction, $\eta(r_{eq})$, of trapped particles given by equation (A18)). The equatorial profile of the CM model is illustrated on Figure 6a by the solid black line as a function of L (or r_{eq}) inside the plasmasphere. As mentioned above, this model is constrained to reproduce the observed electron density profile of CA92 given by equation (A20) inside the plasmasphere. We use the same parameter values as in Figure 2, and we take into account the *Kp*-dependent convection to determine the position of the plasmapause. Note that the density distribution inside the plasmasphere is independent of MLT and of *Kp*, contrary to the plasmapause position. The density observations show only small longitudinal (MLT) dependence [*Clilverd et al.*, 2007].

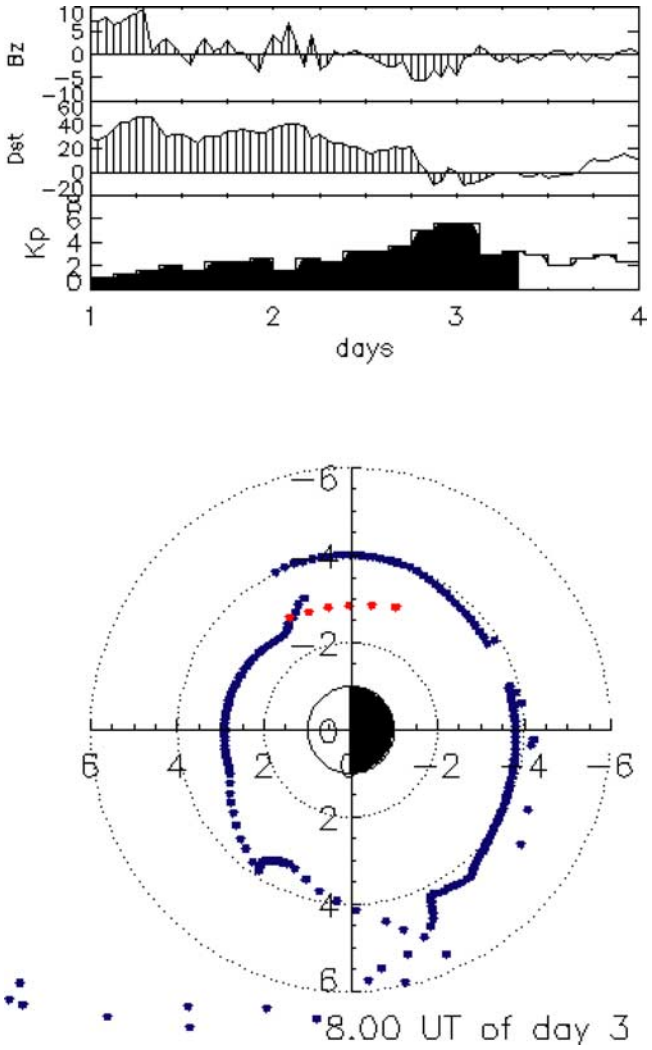

Figure 5a. Result of the dynamic kinetic model in the geomagnetic equatorial plane on 10 June 2001 at 0800 UT. (top) B_z, *Dst*, and *Kp* index from 8 June 2001 at 0000 UT to 10 June 2001 at 2400 UT. (bottom) The blue dots correspond to the position of the plasmapause. The red dots represent the positions of the vestigial plasmapause, since refilling appears after the substorm.

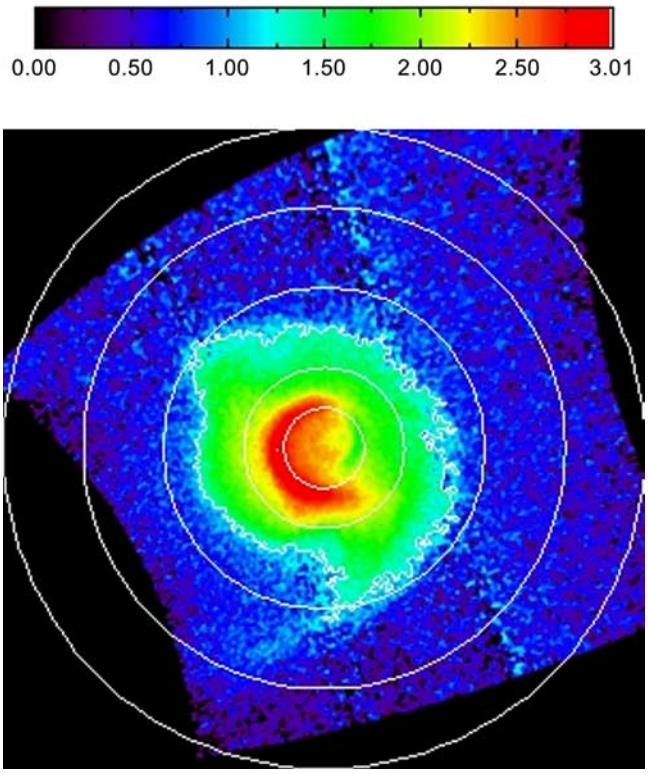

Figure 5b. Observation of EUV/IMAGE on 10 June 2001 at 0805 UT, projected in the geomagnetic equatorial plane. The white circles correspond respectively to L = 2, 4, 6, and 8 R_E.

[45] The positions of the inner and outer edges of the plasmapause region are determined by the dynamic simulation and correspond to the red and black dots on Figure 4a for 8 June 2001 at 1300 UT. At that time, the inner and outer edges are located at the same radial distance corresponding to 4.5 R_E in the 1800 MLT sector. On Figure 6, we show the results obtained on 8 June 2001 at 0900 UT in the 1800 MLT sector. The inner and outer edges are then respectively 4.1 and 4.4 R_E. The density in the plasmapause region between the inner and outer edges is a linear extrapolation (in logarithmic scale) of the plasmaspheric and the plasma trough density values at these edges. The number density profile in the plasmatrough is a generalization of the empirical function of L [*Carpenter and Anderson*, 1992], depending on the MLT angle and given in Appendix A of the present paper.

[46] The plasmatrough model corresponds quite well to number density profile observed by Cluster on 8 June 2001 from 0600 to 0902 UT in the dusk sector and illustrated by the blue dotted-dashed line on Figure 6a. The four Cluster satellites have a perigee at 4 R_E, so that they do not penetrate often inside the plasmasphere. But their observations are very useful to compare the plasmapause positions and the plasmatrough profiles with model results in this region. The instrument WHISPER (Waves of High frequency and Sounder for Probing of Electron density by Relaxation) measures the total electron density via the relaxation sounder, an active radio frequency technique. The blue dotted-dashed line of Figure 6a shows the average equatorial density determined from the measurements of the four spacecraft during their orbit from 0600 to 0902 UT on 8 June 2001 between 1713 and 1809 MLT. The steeper slope of the density profile between L = 4 and 5 indicates that the observed position of the plasmapause is slightly further to Earth and decreases more slowly than what is predicted by the dynamic model. The number density given by the model inside the plasmasphere is several times larger than the density measured by Cluster just below the plasmapause. Despite the 48 h period before 8 June 2001 was relatively quiet, Cluster observations show that the number density at L = 4 R_E is still well below saturation.

[47] In addition to EUV observations, IMAGE has also provided measurements of the electron number density on 8 June 2001 with the Radio Plasma Imager (RPI). This sounding instrument working in the frequency range from 3 kHz to 3 MHz is able to determine the electron density distribution along the magnetic field line that intersects the spacecraft [*Reinisch et al.*, 2001]. *Huang et al.* [2004] have analyzed the observations of RPI on 8 June 2001 when IMAGE was between L = 2.22 and L = 3.23 in the morning local time sector. An empirical mathematical function was used to fit their observations. The equatorial densities determined by this technique for this period of time are shown by the magenta line made of crosses on Figure 6a. It can be seen that the number density determined in this case by RPI for $L < 3$ is larger than the profile obtained with the model in the inner plasmasphere.

[48] For comparison, the result of an EE model (i.e., a purely exospheric equilibrium model without any trapped population given by equation (A15)) is also plotted in Figure 6a (the dashed black line in the inner plasmasphere). Its exobase altitude is assumed to be 2000 km, the exobase proton and electron densities are equal to $n(r_0) = 24500\ \mathrm{cm}^{-3}$, the electron and proton temperatures are also the same T = 3000 K, and the kappa indices for the both particle species are identical: $\kappa_e = \kappa_p = 100$. This model is in better agreement with RPI observations at low altitudes for $L <$ 3 and with CA92 saturated density profiles at larger radial distances.

[49] The full range equatorial density profile corresponding to the model of *Carpenter and Anderson* [1992] including the inner plasmasphere, the plasmapause region and the plasmatrough region is illustrated by the triple dots-dashed blue line in Figure 6b. The innermost edge of the plasmapause region is determined by a Kp-dependent relation in CA92: Lpp = 5.6–0.46 $Kp_{\max}$. It is located at larger radial distances than the positions predicted by our kinetic model (black line on Figure 6a).

[50] Larger ion densities at smaller radial distances compared to CA92 are obtained by *Gallagher et al.* [2000]. These authors developed an empirical 3-D model called GCPM (Global Core Plasma Model) on the basis of averaged DE1/RIMS (Dynamics Explorer 1/Retarding Ion Mass Spectrometer) observations. The average quiet profile deduced from these DE1 observations is given in equation (A21). The equatorial electron density profile predicted below 650 km is obtained from IRI (International Reference Ionosphere) model. The model covers a larger range of altitudes.

[51] The results of the GCPM model for 8 June 2001 at 0900 UT are illustrated on Figure 6b by the red solid line in

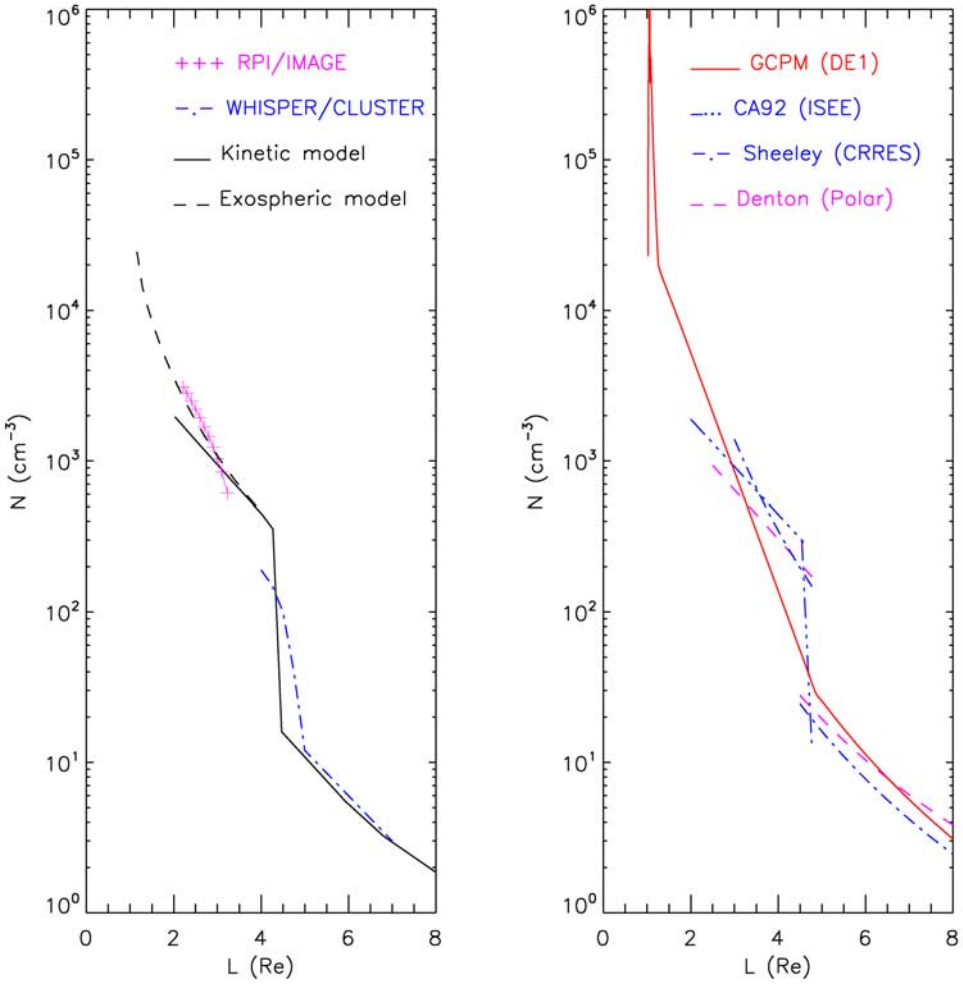

Figure 6. (a) Equatorial profiles of number density obtained from satellite observations and kinetic models developed in the present paper for the date of 8 June 2001. Models are represented by the black solid line, which is the result of the kinetic constrained models (CM) model with a population of trapped particles adjusted on CA92 and a dynamic plasmapause at 0900 UT and in the 1800 MLT sector, and the black dashed line, which is the purely exospheric equilibrium (EE) model with $n(r_0) = 24500$ cm^{-3}. Observations are represented by the magenta line made of crosses, which is the empirical model deduced in the geomagnetic equatorial plane from radio plasma imager (RPI) observations on 8 June 2001 in the morning side [*Huang et al.*, 2004], and the blue dashed-dotted line, which is the averaged Cluster observations on 8 June 2001 from 0600 to 0902 UT in the dusk sector (1713–1809 MLT). (b) Empirical equatorial models deduced from satellite observations. Red line is the global core plasma model (GCPM) of *Gallagher et al.* [2000] on 8 June 2001 at 0900 UT and 1800 MLT. Blue triple dots-dashed line is the model of *Carpenter and Anderson* [1992] with plasmapause obtained for 8 June 2001 at 0900 UT and 1800 MLT. Blue dashed-dotted line is the averaged model obtained in the plasmasphere and the plasmatrough from CRRES observations [*Sheeley et al.*, 2001]. Magenta dashed line is the averaged model obtained in the plasmasphere and the plasmatrough from Polar observations [*Denton et al.*, 2004].

1800 MLT. Note the rather significant differences with the model CA92 (blue triple dots-dashed line). For $L < 2.6$, *Carpenter and Anderson* [1992] found saturated plasmaspheric densities below that of the GCPM model. At $L = 2$, the CA92 equatorial number density is 3 times smaller than the value given by the GCPM. On the contrary, at $L = 4$ (immediately below the inner edge of the plasmapause region), the CA92 density is four times larger than predicted by the GCPM. Note that GCPM is determined from DE1 ion measurements made during quiet periods while CA92 was obtained using ISEE1 saturated electron density profiles during very quiet prolonged periods only and for a different phase of the solar cycle.

[52] Other average equatorial profiles have been obtained from CRRES observations [*Sheeley et al.*, 2001] and from Polar [*Denton et al.*, 2004]. Their expressions are respectively given by equations (A22) and (A23) inside the plasmasphere and equations (A40) and (A41) in the plasmatrough. These profiles are reported on Figure 6b. Significant differences are obtained between all these empirical models,

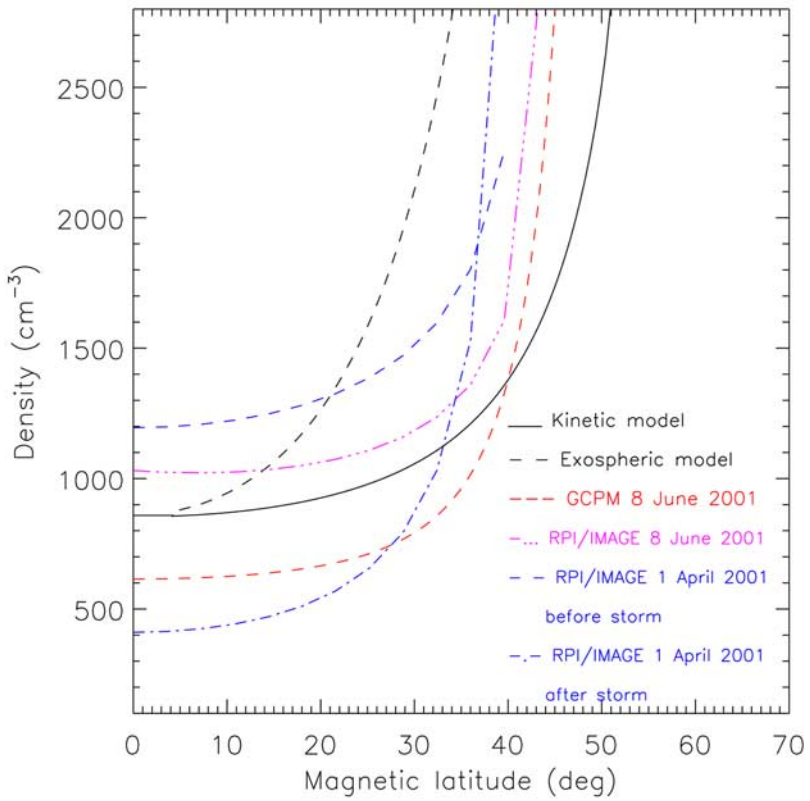

Figure 7. Latitudinal dependence of the number density profiles on 8 June 2001 compared with RPI observations and GCPM model. Magenta triple dots-dashed line is the observation of RPI on 8 June 2001 along the $L = 3$ flux tube [*Huang et al.*, 2004]. Blue lines are the observation of RPI on 1 April 2001 along a $L = 2.84$ flux tube, before the storm (dashed line) and after the storm (dashed-dotted line) [*Tu et al.*, 2006]. Solid black line is our kinetic model along an $L = 3$ flux tube with an adjusted population of trapped particles constrained to fit the average CA92 equatorial density profile for prolonged quiet conditions. Dashed black line is the purely exospheric EE model along the $L = 3$ flux tube for an exobase at 2000 km with same equatorial densities as our kinetic model. Red dashed line is the GCPM Model on 8 June 2001 along the $L = 3$ flux tube [*Gallagher et al.*, 2000] at 1800 MLT.

because of different characteristics of the observation instruments, different orbits and different methods used to select the data during quiet periods in the inner plasmasphere. Polar made measurements far from the equator. GCPM is based on ion particle observations from DE1 Plasma Wave Instrument and shows an equatorial profile quite different from the others. Among all these observations, we chose the equatorial profile of *Carpenter and Anderson* [1992] as the best one to constrain our model in the inner plasmasphere since it is based on ISEE measurements of the electron number density at low latitude.

[53] The slight annual, semiannual and solar cycle variations discovered by *Carpenter and Anderson* [1992] in the ISEE1 observations are also taken into account to constrain the kinetic model (see Appendix A). The amplitudes of these variations are small and have effects mainly at smallest radial distances. The plasmaspheric density is larger in December than in June. It is also larger at solar maximum than at solar minimum.

4.2. Latitudinal Profiles

[54] The latitudinal dependence of the model and of some RPI observations is illustrated on Figure 7. The magenta triple dots-dashed line illustrates the observations of RPI collected on 8 June 2001 along an $L = 3$ flux tube in the morning MLT sector [*Huang et al.*, 2004]. The blue lines show observations of RPI on 1 April 2001 along $L = 2.84$ flux tube before a storm (dashed line) and after the storm (dashed-dotted line) [*Tu et al.*, 2006], when the flux tube has been depleted. It can be seen that the observed profiles are very flat in the equatorial region, especially during geomagnetically quiet periods when the flux tubes are expected to be populated with a significant amount of trapped particles. The field-aligned density distributions have much steeper gradients at higher latitudes, i.e., at lower altitudes.

[55] The red dashed line on Figure 7 corresponds to the result of the GCPM Model on 8 June 2001 along the $L = 3$ flux tube [*Gallagher et al.*, 2000] at 1800 MLT. This plasmaspheric profile has also little variations at middle and low latitudes but significant variations at higher latitudes.

[56] The black dashed line corresponds to the latitudinal density profile along an $L = 3$ magnetic flux tube for the near Maxwellian EE model quoted above. It can be seen that this fully collisionless density distribution increases with the latitude much more steeply than the densities

derived from the RPI observations. This is evidence that, at least in saturated flux tube, there is a larger abundance of trapped particles of the classes C and E in addition to the ballistic, escaping and incoming particles of classes A, B, and D.

[57] The solid black line shows the field aligned density for our kinetic model with trapped particles constrained by the CA92 equatorial density. At low latitudes, this kinetic model including a fraction of trapped particles gives flatter density profiles which are in better agreement with the RPI results. This confirms that the presence of trapped particles in the kinetic model provides a more realistic latitudinal density distribution than the purely collisionless EE model. Trapped particles are necessary to obtain a latitudinal dependence corresponding to the RPI observations. Nevertheless, the number density observed along the $L = 3$ magnetic flux tube on 8 June 2001 is higher than that of CA92 and therefore of that of our kinetic model.

[58] The kinetic model described here could be improved by constraining the number of trapped particles by other equatorial density profiles than that of CA92. It is clear that by using exobase densities, temperatures and kappa indexes that are not identical in both hemispheres or/and that would be functions of the invariant latitude, as well as of the MLT of the magnetic field lines, it might be possible to fit almost any observed radial and MLT distributions of the density distribution. Furthermore, by allowing η, the fraction of trapped particles, to be also a fit function of λ, the magnetic latitude, it would be possible to fit almost any observed field-aligned plasma density distributions like those determined by *Reinisch et al.* [2001] and *Tu et al.* [2006] from the RPI/IMAGE measurements.

5. Other Moments of the Velocity Distribution

[59] One of the key advantages of kinetic models like that outlined above, is that it provides not only the distribution of electron and ions number densities, but can offer also other physical quantities corresponding to the higher-order moments of the VDFs for all these particle species. The field aligned and equatorial distributions of the electron and proton temperature are especially of interest to test and improve such kinetic models. This is not the case for empirical models based on arbitrary mathematical fit functions ungrounded on physical principles. The equatorial proton temperature profiles in such a kinetic model has been determined and discussed in the paper of *Pierrard and Lemaire* [2001]. They showed that the equatorial proton and electron temperatures are much more sensitive to the value adopted for the index kappa of the VDF than the density which corresponds to its zero-order moment. The kappa value has only a small influence on the density profiles, but it is crucial for the temperature profiles [*Pierrard and Lemaire*, 2001]. The smaller the value of the index kappa, the larger is the positive temperature gradient along magnetic field lines in a diffusive equilibrium model. The index κ cannot be smaller than 2 so that all the physical moments of the VDF can be calculated. The case $\kappa = 2$ with a model in diffusive equilibrium appears thus as the maximum increase for the temperature profile at the equator, given by $T(r) = T_0 \frac{\kappa}{\kappa - 3/2} \left(1 + \frac{q(r)}{\kappa}\right)$, where the different variables are defined in Appendix A. Note that the temperatures observed nightside and dayside can be quite different and vary from 3000 to more than 5000 K [*Bezrukikh et al.*, 2003].

[60] On the contrary, in the case of a model in exospheric equilibrium, the temperature decreases with altitude. A variable fraction of trapped particles in magnetic flux tubes can possibly be used to fit future observed field-aligned ion and electron temperature distributions in the plasmasphere and plasmatrough.

[61] Note that all the plasmaspheric models presented in this paper (DE, EE, CM) were assumed to be in equilibrium. The fraction of incoming particles (represented by ξ in equation (A1)) was assumed to be equal to 1 so that the flux of escaping particles is exactly equal to the flux of escaping particles. But the models can also account for the presence of an escape flux by assuming that there are less incoming particles of class B than escaping particles of the class A. In this case, the fraction of incoming particles is $\xi < 1$. Such kinetic models can then be used to simulate a plasmaspheric wind (see equation (A16)) and therefore account for the absence of plasmapause as observed after prolonged very quiet periods [*Lemaire and Schunk*, 1992]. By adjusting the fraction of incoming particles compared to the escaping one, any net field aligned flux can be obtained to feed the cross-L expansion of the plasmaspheric wind. The polar wind reviewed by *Lemaire and Pierrard* [2001] is an extreme case of this sort of kinetic model of the plasmaspheric wind, where the population of incoming particles is assumed to be empty along open field lines: $\xi = 0$ (see equation (A17)).

[62] To evaluate the fractions of the different classes of electrons and ions in their VDFs, the Fokker-Planck equation can be solved like in the work of *Pierrard and Lemaire* [1998]. But these future developments are beyond the grasp of this simple kinetic model of the plasmasphere and plasmatrough.

6. Conclusions

[63] In this paper, we developed a 3-D kinetic model of the plasmasphere that is constrained by realistic data. Unlike some other empirical models, the model outlined above is based on physical grounds and uses the kinetic approach to determine the moments of the particles inside the plasmasphere. The model is three-dimensional and allows us to compare with equatorial and field aligned density profiles from various sources of observations, like RPI and EUV on IMAGE or WHISPER on Cluster. The kinetic model is constrained by observations that can be improved in the future versions to give even more comprehensive density distributions both in the equatorial plane and along magnetic field lines.

[64] The model presented above is also a dynamic one since it takes into account the variations of the geomagnetic activity level to determine the position and the thickness of the plasmapause. It can easily be extended by allowing the VDFs to be asymmetrical with respect to the northern and southern exobases as well as a as function of the MLT angle. The model of plasmatrough can also be improved in the future by using Cluster observations. Similar kinetic approaches have been used to model other related regions of the magnetosphere like the polar wind [*Pierrard and Lemaire*, 1996] and the auroral regions [*Pierrard*, 1996]. They can be merged into future versions of our kinetic

model outlined above exclusively for the plasmasphere and plasmatrough.

Appendix A

[65] In this appendix, we present the equations used in the different kinetic models.

A1. Classes of Particles

[66] The total number density n_{tot} is given by the sum

$$n_{tot} = n_{ball} + n_{esc} + \zeta n_{inc} + \eta n_{trp}, \tag{A1}$$

where n_{ball}, n_{esc}, n_{inc}, and n_{trp} are respectively the number density of the ballistic, escaping, incoming and trapped particles.

[67] Using the same process as that used by *Pierrard and Lemaire* [1996] but for a model of plasmasphere along closed field lines, we obtain

$$n_{ball} = n_0\left(1+\frac{q(r)}{\kappa}\right)^{-\kappa-1} \cdot \left[d^{3/2}(1-\beta_2(b)) - \alpha c^{3/2}(1-\beta_2(f))\right], \tag{A2}$$

$$n_{esc} = n_0\left(1+\frac{q(r)}{\kappa}\right)^{-\kappa-1}\frac{1}{2}\left[d^{3/2}\beta_2(b) - \alpha c^{3/2}\beta_2(f)\right], \tag{A3}$$

$$n_{inc} = n_{esc}, \tag{A4}$$

$$n_{trp} = n_{classes\,C+E} = n_0\left(1+\frac{q(r)}{\kappa}\right)^{-\kappa-1}\alpha c^{3/2}, \tag{A5}$$

where

$$d = \left(1+\frac{q(r)}{\kappa}\right), \tag{A6}$$

$$\alpha = p^{1/2}\left(1+\frac{B(r)q(r)}{B(r_0)p(\kappa+q(r))}\right)^{-\kappa-1}, \tag{A7}$$

$$c = 1+\frac{q(r)}{p\kappa}, \tag{A8}$$

$$p = 1-\frac{B(r)}{B(r_0)}, \tag{A9}$$

$$\beta_2(x) = \int_0^x \frac{\Gamma(\kappa+1)}{\Gamma(\kappa-1/2)\Gamma(3/2)} t^{\kappa-3/2}(1-t)^{1/2}dt, \tag{A10}$$

where Γ is the Gamma function,

$$b = \left(1+\frac{V_\infty^2}{\kappa+q}\right)^{-1}, \tag{A11}$$

$$f = \left(1+\frac{X^2}{p\kappa+q}\right)^{-1},$$

$$V_\infty^2(r) = \frac{-m\Phi_g(r) + \frac{1}{2}m\Omega^2 r^2\cos^2\lambda - ZeV(r)}{kT_0}, \tag{A12}$$

$$X^2(r) = pV_\infty^2(r) - \frac{B_0(r)}{B_0(r_0)}q(r), \tag{A13}$$

Here n_0 is the number density at the exobase radial distance r_0, κ is the kappa index ($2 < \kappa$), $B(r)$ is the magnetic field, $q(r)$ is given in equation (A24), and n_{ball} and n_{esc} are similar to equations (A5) and (A25) as obtained by *Pierrard and Lemaire* [1996] for open field lines and using the same notation.

A2. Types of Kinetic Models

[68] Different models can be obtained depending on the values of the parameters ζ and η controlling respectively the number of incoming and trapped particles. Models with $\zeta = 1$ are in hydrostatic equilibrium (no flux) while the other models are characterized by an escape flux (wind).

Model (DE) in diffusive equilibrium (n_{diff}): $\zeta = 1$ and $\eta = 1$

$$n_{diff} = n_0\left(1+\frac{q(r)}{\kappa}\right)^{-\kappa+1/2} \tag{A14}$$

Model (EE) in exospheric equilibrium (n_{exo}): $\zeta = 1$ and $\eta = 0$

$$n_{exo} = n_{diff} - n_{trp}, \tag{A15}$$

where n_{diff} is given by equation (A14) and n_{trp} by equation (A5). These expressions avoid calculations of β_2 functions.

Model with plasmaspheric wind

$$0 < \zeta < 1 \tag{A16}$$

Model of polar wind

$$\zeta = 0 \text{ and } \eta = 0 \tag{A17}$$

Model (CM) in hydrostatic equilibrium constrained (n_{constr}) to fit an observed profile (n_{obs}) by considering a fraction of trapped particles: $\zeta = 1$ and

$$\eta(L) = \frac{n_{obs}(L) - n_{exo}(L)}{n_{diff}(L) - n_{exo}(L)} \tag{A18}$$

$$n_{constr} = n_{exo} + \eta n_{trp} \tag{A19}$$

Saturated plasmaspheric profile deduced from ISEE1 [*Carpenter and Anderson*, 1992]

$$\log_{10} n_{obs} = (-0.3145L + 3.9043) + D$$
$$D = \left[0.15\left(\cos\frac{2\pi(d+9)}{365} - 0.5\cos\frac{4\pi(d+9)}{365}\right) + 0.00127S - 0.0635\right]\exp\left(\frac{-(L-2)}{1.5}\right), \tag{A20}$$

where d is the number of the day, S is the 13-month average sunspot number, and L is the McIlwain parameter.

Average quiet profile deduced from DE1/RIMS [*Gallagher et al.*, 2000]

$$\log_{10} n_{\rm obs} = (-0.79L + 5.3) + D. \tag{A21}$$

The average number density (in $\rm cm^{-3}$) in the plasmasphere as a function of L shell found with CRRES observations is given by [*Sheeley et al.*, 2001]

$$n_{\rm obs} = 1390\left(\frac{3}{L}\right)^{4.8} \pm 440\left(\frac{3}{L}\right)^{3.6} \text{ for } 3 < L < 7. \tag{A22}$$

The equatorial average plasmaspheric density determined from Polar observations is given by [*Denton et al.*, 2004]

$$\log_{10} n_{\rm obs} = -0.324L + 3.78 + D. \tag{A23}$$

A3. Potential

[69] The gravitation, the centrifugal and the electric potentials are taken into account

$$q(r) = \frac{-m\Phi_g(r_0) - \frac{1}{2}m\Omega^2 r_0^2 \cos^2\lambda - \mathrm{Ze}V(r_0) + m\Phi_g(r) + \frac{1}{2}m\Omega^2 r^2 \cos^2\lambda + \mathrm{Ze}V(r)}{kT_0}. \tag{A24}$$

The gravitational potential is given by

$$\Phi_g(r) = \frac{GM_E}{r}, \tag{A25}$$

where G = 6.6726 10^{-11} $\rm m^3\ s^{-2}\ kg^{-1}$ is the gravitational constant, M_E = 5.976 10^{24} kg is the mass of the Earth, m is the mass of the particle species, Ze their charge, T_0 their temperature at the exobase, λ is the geomagnetic latitude. Ω is the local angular velocity of the plasma and corresponds to 7.29 10^{-5} rad $\rm s^{-1}$ in case of Earth corotation: $\Omega = \Omega_E$.

[70] For all models without any flux (exospheric, diffusive equilibrium, plasmaspheric with $\zeta = 0$), the electrostatic potential is given by Pannekoek-Rosseland [*Pierrard and Lemaire*, 1996]

$$eV(r) = -\frac{\sum\limits_j Z_j m_j n_j / kT_j}{\sum\limits_j Z_j^2 n_j / kT_j}\Phi_g(r). \tag{A26}$$

For a plasma with electrons and protons having the same temperature and the same density for quasi-neutrality,

$$V(r) = -\frac{m_p - m_e}{2e}\Phi_g(r). \tag{A27}$$

To obtain the model in 3-D, $n_{\rm tot}$ is calculated along the field line L. The $\eta(L)$ and $n(L)$ are determined from the fit with $n_{\rm obs}$ in the geomagnetic equator and determine $n(r_0)$.

A4. Plasmapause

[71] The radial distance of the ZPFS in the geomagnetic equator is given by

$$L_Z = \left(\frac{2GM_E}{3\Omega^2 R_E}\right)^{1/3} = 5.78\left(\frac{\Omega_E}{\Omega}\right)^{2/3}. \tag{A28}$$

The drift velocity is given by

$$\frac{\vec{E}\times\vec{B}}{B^2} \tag{A29}$$

and the angular drift velocity is given by

$$\Omega(r) = \frac{\left|\left(\vec{E}_{\rm tot}\times\vec{B}\right)\times\vec{r}\right|}{r^2 B^2}. \tag{A30}$$

A5. Magnetic field

[72] The dipole magnetic field is given by

$$B(r,\lambda) = \frac{M}{r^3}\left(1 + 3\sin^2\lambda\right)^{1/2}, \tag{A31}$$

where M = 8 10^{15} $\rm Tm^3$ is the dipolar magnetic moment of the Earth. Equation of dipole magnetic field line

$$r = L\cos^2\lambda. \tag{A32}$$

A6. Total Electric Field $\mathbf{E_{tot}}$ (Convection and Corotation)

[73] The total electric field: $\vec{E} = -\nabla\phi$ where φ is the total electric potential. The Kp-dependent convection E5D electric potential in kV [*McIlwain*, 1986] with corotation is given by

$$\phi = \{r[0.8\sin(\theta) + 0.2\cos(\theta)] + 3\}(1 + 0.3K_r)H - \frac{92}{r}, \tag{A33}$$

where r is the radial distance, θ the magnetic longitude (= 15° × MLT)

$$K_r = \frac{K_p}{1 + 0.1K_p}, \tag{A34}$$

Kp is the geomagnetic index, and

$$H = \frac{1}{1 + (0.8R_{\rm ar}/r)^8}. \tag{A35}$$

Location of the auroral ring (in R_E)

$$R_{ar} = 9.8 - 1.4\cos\theta - (0.9 + 0.3\cos\theta)K_r. \tag{A36}$$

A7. Plasmatrough

[74] Plasmatrough profiles of electrons are taken from *Carpenter and Anderson* [1992]

$$n_e(r) = (5800 + 300t)L^{-4.5} + \left[1 - e^{-(L-2)/10}\right] \text{ for } 0 \leq t < 6 \text{ MLT}, \quad \text{(A37)}$$

$$n_e(r) = (-800 + 1400t)L^{-4.5} + \left[1 - e^{-(L-2)/10}\right] \text{ for } 6 \leq t \leq 15 \text{ MLT}. \quad \text{(A38)}$$

We complete by

$$n_e(r) = (-800 + 1400 * 12)L^{-4.5} + \left[1 - e^{-(L-2)/10}\right] \text{ for } 15 \leq t \leq 24 \text{ MLT}. \quad \text{(A39)}$$

From CRRES observations, *Sheeley et al.* [2001] deduced in the plasmatrough

$$n_e = 124\left(\frac{3}{L}\right)^{4.} \pm 78\left(\frac{3}{L}\right)^{4.72} \text{cm}^{-3}. \quad \text{(A40)}$$

From Polar observations, *Denton et al.* [2004] found in the plasmatrough

$$\log_{10}(n_e) = (-3.45 \pm 0.41)\log_{10}(L) + (3.77 \pm 0.31). \quad \text{(A41)}$$

[75] **Acknowledgments.** The authors thank the director of IASB-BIRA as well as the Belgian SSTC for their support. They also thank J. Lemaire for his detailed reading of this paper and for his advice. The authors thank also D. Gallagher for providing the results of the GCPM model and F. Darrouzet for the Cluster observation on 8 June 2001.

[76] Amitava Bhattacharjee thanks Heinz Wiechen and another reviewer for their assistance in evaluating this manuscript.

References

Baker, D. N., S. G. Kanekal, X. Li, S. P. Monk, J. Goldstein, and J. L. Burch (2004), An extreme distortion of the Van Allen belt arising from the "Halloween" storm in 2003, *Nat.*, *432*, 878–881, doi:10.1038/nature03116.

Bezrukikh, V. V., G. A. Kotova, L. A. Lezhen, J. Lemaire, V. Pierrard, and Y. I. Venediktov (2003), Dynamics of temperature and density of cold protons of the Earth's plasmasphere measured by the Auroral Probe/Alpha-3 experiment data during geomagnetic disturbances, *Cosmic Res. Engl. Transl.*, *41*(4), 392–402, doi:10.1023/A:1025013828230.

Bilitza, D., K. Rawer, L. Bossy, and T. Gulyaeva (1993), International Reference Ionosphere- Past, present and future, *Adv. Space Res.*, *13*, 3–13, doi:10.1016/0273-1177(93)90240-C.

Carpenter, D. L., and R. R. Anderson (1992), An ISEE/whistler model of equatorial electron density in the magnetosphere, *J. Geophys. Res.*, *97*(A2), 1097–1108, doi:10.1029/91JA01548.

Clilverd, M. A., N. P. Meredith, R. B. Horne, S. A. Glauert, R. R. Anderson, N. R. Thomson, F. W. Menk, and B. R. Sandel (2007), Longitudinal and seasonal variations in plasmaspheric electron density: Implication for electron precipitation, *J. Geophys. Res.*, *112*, A11210, doi:10.1029/2007JA012416.

Dandouras, I., et al. (2005), Multipoint observations of ionic structures in the Plasmasphere by Cluster-CIS and comparisons with IMAGE-EUV observations and with model simulations, in *Inner Magnetosphere Interactions: New Perspectives From Imaging*, *Geophys. Monogr. Ser.*, vol. 159, edited by J. Burch, M. Schulz, and H. Spence, pp. 23–54, AGU, Washington, D. C., doi:10.1029/159GM03.

Darrouzet, F., et al. (2006), Analysis of plasmaspheric plumes: Cluster and IMAGE observations, *Ann. Geophys.*, *24*, 1737–1758.

Denton, R. E., J. D. Menietti, J. Goldstein, S. L. Young, and R. R. Anderson (2004), Electron density in the magnetosphere, *J. Geophys. Res.*, *109*, A09215, doi:10.1029/2003JA010245.

Gallagher, D. L., P. D. Craven, and R. H. Comfort (2000), Global core plasma model, *J. Geophys. Res.*, *105*, 18,819–18,833, doi:10.1029/1999JA000241.

Goldstein, J., J. L. Burch, and B. R. Sandel (2005a), Magnetospheric model of subauroral polarization stream, *J. Geophys. Res.*, *110*, A09222, doi:10.1029/2005JA011135.

Goldstein, J., S. G. Kanekal, D. N. Baker, and B. R. Sandel (2005b), Dynamic relationship between the outer radiation belt and the plasmapause during March–May 2001, *Geophys. Res. Lett.*, *32*, L15104, doi:10.1029/2005GL023431.

Huang, X., B. W. Reinisch, P. Song, J. L. Green, and D. L. Gallagher (2004), Developing an empirical density model of the plasmasphere using IMAGE/RPI observations, *Adv. Space Res.*, *33*, 829–832, doi:10.1016/j.asr.2003.07.007.

Lemaire, J. (1976), Rotating ion exospheres, *Planet. Space Sci.*, *24*, 975–985.

Lemaire, J. (1989), Plasma distribution models in a rotating magnetic dipole and refilling of plasmaspheric flux tubes, *Phys. Fluids B*, *1*, 1519, doi:10.1063/1.858928.

Lemaire, J. F., and K. I. Gringauz (1998), *The Earth's Plasmasphere*, 350 pp., Cambridge Univ. Press, Cambridge, U. K.

Lemaire, J., and V. Pierrard (2001), Kinetic models of solar and polar winds, *Astrophys. Space Sci.*, *277*(1/2), 169–180, doi:10.1023/A:1012245909542.

Lemaire, J., and R. W. Schunk (1992), Plasmaspheric wind, *J. Atmos. Terr. Phys.*, *54*, 467–477, doi:10.1016/0021-9169(92)90026-H.

Maksimovic, M., V. Pierrard, and P. Riley (1997), Ulysses electron distributions fitted with Kappa functions, *Geophys. Res. Lett.*, *24*(9), 1151–1154, doi:10.1029/97GL00992.

McIlwain, C. E. (1986), A *Kp* dependent equatorial electric field model, *Adv. Space Res.*, *6*(3), 187–197, doi:10.1016/0273-1177(86)90331-5.

Ober, D., J. Horwitz, and D. Gallagher (1997), Formation of density troughs embedded in the outer plasmasphere by subauroral ion drift events, *J. Geophys. Res.*, *102*(A7), 14,595–14,602, doi:10.1029/97JA01046.

Pierrard, V. (1996), New model of magnetospheric current-voltage relationship, *J. Geophys. Res.*, *101*, 2669–2675, doi:10.1029/95JA00476.

Pierrard, V. (2006), The dynamics of the plasmasphere, in *Space Science: New Research*, edited by S. Nick Maravell, pp. 83–96, Nova Sci., Hauppauge, N. Y., ISBN: 1-60021-005-8.

Pierrard, V., and J. Cabrera (2005), Comparisons between EUV/IMAGE observations and numerical simulations of the plasmapause formation, *Ann. Geophys.*, *23*(7), 2635–2646, SRef-ID: 1432–0576/ag/2005–23–2635.

Pierrard, V., and J. Cabrera (2006), Dynamical simulations of plasmapause deformations, *Space Sci. Rev.*, *122*(1–4), 119–126, doi:10.1007/s11214-006-5670-3.

Pierrard, V., and J. Lemaire (1996), Lorentzian ion exosphere model, *J. Geophys. Res.*, *101*, 7923–7934, doi:10.1029/95JA03802.

Pierrard, V., and J. Lemaire (1998), A collisional kinetic model of the polar wind, *J. Geophys. Res.*, *103*(A6), 11,701–11,709, doi:10.1029/98JA00628.

Pierrard, V., and J. Lemaire (2001), Exospheric model of the plasmasphere, *J. Atmos. Sol. Terr. Phys.*, *63*(11), 1261–1265, doi:10.1016/S1364-6826(00)00227-3.

Pierrard, V., and J. Lemaire (2004), Development of shoulders and plumes in the frame of the interchange instability mechanism for plasmapause formation, *Geophys. Res. Lett.*, *31*(5), L05809, doi:10.1029/2003GL018919.

Pierrard, V., G. V. Khazanov, J. Cabrera, and J. Lemaire (2008), Influence of the convection electric field models on predicted plasmapause positions during the magnetic storms, *J. Geophys. Res.*, *113*, A08212, doi:10.1029/2007JA012612.

Reinisch, B. W., X. Huang, P. Song, G. S. Sales, S. F. Fung, J. L. Green, D. L. Gallagher, and V. M. Vasyliunas (2001), Plasma density distribution along the magnetospheric field: RPI observations from IMAGE, *Geophys. Res. Lett.*, *28*(24), 4521–4524, doi:10.1029/2001GL013684.

Schaefer, S., K. H. Glassmeier, P. T. I. Eriksson, V. Pierrard, K. H. Fornaçon, and L. G. Blomberg (2007), Spatial and temporal characteristics of poloidal waves in the terrestrial plasmasphere: A Cluster case study, *Ann. Geophys.*, *25*, 1011–1024.

Sheeley, B. W., M. B. Moldwin, H. K. Rassoul, and R. R. Anderson (2001), An empirical plasmasphere and trough density model: CRRES observations, *J. Geophys. Res.*, *106*(A11), 25,631–25,641, doi:10.1029/2000JA000286.

Tu, J.-N., J. L. Horwitz, P. Song, X.-Q. Huang, B. W. Reinisch, and P. G. Richards (2003), Simulating plasmaspheric field-aligned density profiles measured with IMAGE/RPI: Effects of plasmasphere refilling and ion heating, *J. Geophys. Res.*, *108*(A1), 1017, doi:10.1029/2002JA009468.

Tu, J., P. Song, B. D. Reinisch, J. L. Green, and X. Huang (2006), Empirical specification of field-aligned plasma density profiles for plasmasphere refilling, *J. Geophys. Res.*, *111*, A06216, doi:10.1029/2005JA011582.

Webb, P. A., and E. A. Essex (2004), A dynamic global model of the plasmasphere, *J. Atmos. Sol. Terr. Phys.*, *66*, 1057–1073, doi:10.1016/j.jastp.2004.04.001.

V. Pierrard and K. Stegen, Belgian Institute for Space Aeronomy, Ringlaan 3, B-1180 Brussels, Belgium. (viviane.pierrard@oma.be)